Supplementary Information (SI) for Materials Chemistry Frontiers.
This journal is © the Partner Organisations 2026

Supplementary information for "A scalable kinetic Monte Carlo platform for charge transport dynamics in polymer-based memristive systems"

Gerliz M. Gutiérrez-Finol,[1] Kirill Zinovjev,[2] Alejandro Gaita-Ariño,[1, *] and Salvador Cardona-Serra[2, †]

[1] *Instituto de Ciencia Molecular (ICMol), Universitat de València, Paterna, Spain*

[2] *Departamento de Química Física, Facultad de Química, Universitat de València, Burjassot, Spain*

(Dated: February 25, 2026)

Contents

* alejandro.gaita@uv.es
† salvador.cardona@uv.es

S1. Device Geometry and Material Parameters

In this section, we describe the structural and physical assumptions used to model the polymer-based memristive device. The aim is to bridge the gap between the experimental configuration and its computational representation, ensuring that the simulated system retains the essential spatial scales, material composition, and boundary conditions of the real device.

To reproduce the experimental behavior of a polymer-based memristive device in simulation, we began with a computationally simple but physically representative model. Rather than attempt to capture the full complexity of coupled ionic–electronic processes, we focused on the motion of cations within the active layer. The polymer matrix and anions are treated implicitly as a fixed background that defines the energy landscape and electrostatic environment for the mobile cations. The following subsections detail the simulated structure, the way it is discretized, and the boundary conditions applied during calculations.

S1.1 Simulated polymer-based memristor structure

The simulated structure follows the experimental device reported by Prado-Socorro et al. [1]. The active layer in the experimental device consists of a composite made of Super Yellow, a polyphenylenevinylene derivative used as the semiconducting host, Hybrane DEO750 8500 as the ion conducting polymer, and lithium triflate ($LiCF_3SO_3$) as the ionic dopant. Together, these materials form a solid state ionic conductor that exhibits memristive behavior.

For the purposes of this simulation, only lithium cations (Li^+) are treated as mobile species. The anions are assumed to remain effectively immobile within the time window of interest, acting as a fixed background charge. This assumption simplifies the model and allows the simulation to focus on the dominant ionic mechanism observed experimentally, namely the migration and accumulation of Li^+ under an applied bias.

S1.2 Lattice Dimensions and Discretization Scheme

The active layer of the simulated device is represented using a two dimensional lattice. The vertical direction corresponds to discrete rails spanning the device thickness, while the horizontal direction represents the available sites along each rail. Each lattice site is interpreted as a possible location for a single cation within a nanoscale region of the polymer matrix.

The total number of cations is chosen to match a given fraction of the available lattice sites, based on the experimental ion concentration. In practice, this concentration reflects the ratio of ionic species to the host polymer matrix, so the occupancy fraction used in the simulator provides a practical way to translate experimental loading levels into the number of mobile ions included in the lattice. This correspondence is approximate, since the lattice is an abstract representation rather than a direct mapping onto individual polymer repeat units. The total number of cations is initially distributed evenly across the vertical rails, resulting in a uniform ion distribution at the start of the simulation. From this initial state, ions are allowed to migrate in response to electric fields, local concentration gradients, and Coulombic repulsion. This approach enables the simulation to capture regimes dominated by drift as well as diffusion.

For typical device dimensions, with a thickness of approximately 200 nm as measured by profilometry, the lattice contains hundreds of cells along the vertical direction and thousands along the lateral direction. This resolution is sufficient to capture both short range hopping events and long range drift and diffusion processes. The spacing between lattice points is chosen so that nearest neighbor interactions provide a reasonable approximation of the microstructure of the blended polymer and ion conducting matrix.

S1.3 Physical Dimensions and Electrode Configuration

The active layer has a thickness of approximately 209 nm, as determined by profilometry, and an effective active area of 0.0825 cm^2, defined by the overlap between the bottom and top electrodes. The simulated geometry mirrors this vertical configuration, with the lower conductive layer acting as the grounded contact and the upper metallic layer serving as the biased electrode, in accordance with the structure described by Prado-Socorro *et al.* [1].

In the simulation, the lateral dimensions are scaled to maintain computational efficiency while preserving enough spatial resolution to resolve heterogeneity in cations motion. This balance allows the model to capture meaningful transport phenomena without incurring the computational expense of atomistic simulations.

S1.4 Boundary Conditions Applied at Electrodes and Edges

At the electrode interfaces, we apply fixed potential (Dirichlet), boundary conditions, with the voltage difference defined by the applied bias in the simulation. This allows cations to accumulate near the electrodes, where they form electric double layers and alter the local electric field, in line with what is observed experimentally. Along the lateral edges, periodic boundary conditions are employed to represent an extended device area and to reduce finite size effects.

S1.5 Table of Physical Constants and Simulation Parameters

Supplementary Table S1 summarizes all the simulation parameters, device settings, and numerical constants used in this work. It includes the general setup, such as temperature, computing device, and the initial spatial distribution of ions, along with the device geometry defined by the grid dimensions. The table also reports the parameters specific to each simulation protocol, including current decay, hysteresis, and learning or forgetting rate. To support reproducibility, each entry lists the parameter name, its value, the corresponding units, and a brief explanation. By simply changing the `simulation_type` parameter, different types of simulations can be performed without modifying other settings. Further information regarding this table and the role of each parameter for the different simulation protocols is provided in subsection S2.2, where we describe the initialization routines used for each simulation type.

Variable	**Value**	**Units**	**Description**
General configurations			
ion_fraction	30	%	Percentage of ions in the system
Temperature	300	K	Temperature of the simulation environment
save	1	-	Flag to save simulation output (1 = yes, 0 = no)
dimension_y	4000	-	Simulation grid size in y-direction (number of rails)
dimension_x	200	-	Simulation grid size in x-direction (number of cups)
starting_mode	100	%	Percentage of sites initially occupied by ions in the spatial grid
simulation_type	1	-	Type of simulation (1=Relaxation decay, 2=Hysteresis, 3=Learning/forgetting rate)
relaxation_time	0.016	s	Characteristic relaxation time
effective_voltage_difference_factor	0.00005	V	Multiplier accounting for voltage effects due to ion–ion repulsion
device	cpu	-	Compute device (cpu or gpu)
Relaxation decay parameters			
constant_voltage	0	V	Constant voltage applied during relaxation decay
polarization_time	5	s	Duration of polarization step
polarization_voltage_applied	5	V	Voltage applied during polarization
total_time	300	s	Total simulation time for relaxation decay
Hysteresis parameters			
maximum_voltage_H	1	V	Maximum voltage applied during hysteresis sweep
minimum_voltage_H	0	V	Minimum voltage applied during hysteresis sweep
sweep_rate	0.25	V/s	Rate of voltage sweep during hysteresis
Learning/forgetting rate parameters			
maximum_voltage	1	V	Maximum voltage applied
minimum_voltage	-1	V	Minimum voltage applied
time_maximum_pulses	5	s	Duration of maximum pulses
time_minimum_pulses	5	s	Duration of minimum pulses
baseline_pulse	0	V	Baseline voltage of pulses
pulses_shape	1	-	Shape type of applied pulses (1 = triangles, 2 = blocks)
pulse_frequency	10	Hz	Frequency of the applied pulses

Supplementary Table S1. Simulation configuration parameters with values, units, and descriptions.

S2. Algorithmic Implementation

The core simulation framework builds on the stochastic update approach introduced by Gutierrez Finol et al. [2], where discrete states evolve probabilistically according to local transition rules derived from physical considerations. In the present work, however, both the physical interpretation and the numerical implementation differ substantially. While the lanthanide nanomagnet study focuses on spin states in molecular scale systems governed by magnetic interactions, our model is designed to capture the drift and diffusion of ions inside a polymer based memristive matrix under an applied electric bias. In this context, the states matrix explicitly represents the instantaneous positions of individual ions on a discrete lattice that mimics the nanoscopic structure of the device. At each Monte Carlo time step, the matrix is updated using transition probabilities that depend on the local electric field, thermally activated backward hops, and hard core exclusion rules that prevent multiple ions from occupying the same site. This approach preserves the computational efficiency and scalability of the original probabilistic bit algorithm, while incorporating a transport model tailored to ionic conduction, charge accumulation, and relaxation phenomena typical of soft matter memristors.

S2.1 Step-by-Step Explanation of the Markov Chain Monte Carlo Framework

This section describes the stochastic ion transport model used in the polymer-based memristor simulations. The approach follows a Markov Chain Monte Carlo (MCMC) scheme in which mobile cations occupy discrete sites on a two-dimensional matrix. Each row acts as a one-dimensional rail that restricts ion motion to the lateral direction, while several rails are stacked vertically to reflect the layered structure of the device. Within a given rail, ions migrate randomly along the horizontal axis. Within a given rail, ions migrate stochastically along the horizontal direction: at each time step, an ion can hop left, hop right, or remain in place, with probabilities determined by the local electric field, temperature, and spatial zone. Vertical motion and hopping between different rails are not included in the present implementation. The main steps of the simulation loop are described below:

1. Initialization

The device geometry is mapped onto a discrete lattice where each occupied site corresponds to the position of a single ion.

- The vertical dimension (y) corresponds to the number of rails (rows).
- The horizontal dimension (x) corresponds to the number of available hopping sites per rail.
- The total number of ions is determined from the experimental ion fraction data and uniformly distributed at the start.

2. Electric-field-dependent energy gap

At each time step, the influence of the applied bias is translated into an *energy gap* per possible hop:

$$\Delta E = \frac{q_{\text{ion}} \cdot \Delta V_{\text{net}} \cdot d_{hop}}{t_{dev}} \tag{1}$$

where:

- q_{ion} is the ionic charge of the ion (e),
- ΔV_{net} is the net potential drop experienced across the device in volts (including the effect of prior ion accumulation),
- d_{hop} is the hop distance between lattice sites (nm),
- t_{dev} is the device thickness (nm).

This converts the electric field effect into an energy gap (ΔE in eV) between forward and backward moves determining their asymmetry.

3. Boltzmann Factor for Thermal Activation

Thermal activation and field effects are incorporated using a Boltzmann factor:

$$B_{zone} = \exp\left(-\frac{\Delta E_{zone}}{k_B T}\right) \tag{2}$$

where k_B is the Boltzmann constant (8.6173×10^{-5} eV/K), T is the absolute temperature, and the subscript *zone* denotes the spatial "zone" index (1 to 10) used to account for lateral inhomogeneities. Each zone has its own B_{zone} value, meaning regions of the device with different field strengths or ion densities will have different directional bias.

4. Directional hopping probabilities

The Boltzmann weighting is combined with a baseline hopping probability P_0, set by material specific diffusion constants and time step scaling, to produce left and right hopping probabilities:

$$P^{(\leftarrow)}_{zone} = \frac{P_0}{1 + B_{zone}} \tag{3}$$

$$P^{(\rightarrow)}_{zone} = B_{zone} \cdot P^{(\leftarrow)}_{zone} \tag{4}$$

These expressions ensure that forward bias increases the probability of hopping in the field direction, while reverse hops remain possible via thermal activation.

5. Spatial Zones and Local Probabilities

The simulated polymer-based memristive device is represented by a discrete lattice of size $N_y \times N_r$, where N_y is the number of horizontal rows ("rails") and N_r is the number of ions per row. The position of each ion is stored in an integer valued matrix:

$$\mathbf{X}(t) \in \mathbb{Z}^{N_y \times N_r}$$

where each element $X_{ij}(t)$ denotes the column index (spatial position) of ion j in row i at time step t.

As it was mentioned before, the lattice is divided into Z vertical zones of equal width, such that the zone index for ion (i, j) is:

$$z_{ij} = \left\lceil \frac{X_{ij}(t)}{L_x/Z} \right\rceil$$

where L_x is the total number of discrete columns in the horizontal direction. Each zone z is associated with a pair of directional hopping probabilities (equations 3 and 4), which are precomputed from Boltzmann statistics that depend on the local electric field.

6. Random Sampling and Exclusion Rules

At each time step, two independent random matrices are generated:

$$R^{(\rightarrow)}_{ij}, \quad R^{(\leftarrow)}_{ij} \sim \mathcal{U}(0, 1)$$

for all $i \in \{1, \dots, N_y\}$ and $j \in \{1, \dots, N_r\}$.

The minimum distances to the nearest occupied neighbor are computed as:

$$\Delta_{ij}^{(\rightarrow)} = X_{i,j+1}(t) - X_{ij}(t), \quad \Delta_{ij}^{(\leftarrow)} = X_{ij}(t) - X_{i,j-1}(t)$$

with appropriate handling of the first and last ions in each row to account for boundary conditions.

A movement is only considered valid if:

$$\Delta_{ij}^{(\rightarrow)} > 1 \quad \text{(for right moves)}, \quad \Delta_{ij}^{(\leftarrow)} > 1 \quad \text{(for left moves)}$$

7. Movement Acceptance and Position Update

Define the movement masks:

$$M_{ij}^{(\rightarrow)} = \begin{cases} 1, & \text{if } R_{ij}^{(\rightarrow)} \leq p_{z_{ij}}^{(\rightarrow)} \text{ and } \Delta_{ij}^{(\rightarrow)} > 1 \\ 0, & \text{otherwise} \end{cases}$$

$$M_{ij}^{(\leftarrow)} = \begin{cases} 1, & \text{if } R_{ij}^{(\leftarrow)} \leq p_{z_{ij}}^{(\leftarrow)} \text{ and } \Delta_{ij}^{(\leftarrow)} > 1 \\ 0, & \text{otherwise} \end{cases}$$

The ion positions are updated according to:

$$X_{ij}(t+1) = X_{ij}(t) + M_{ij}^{(\rightarrow)} - M_{ij}^{(\leftarrow)}$$

This procedure is applied simultaneously to all ions, ensuring a parallel Monte Carlo update at each iteration. In summary, for each ion:

1. A random number $r^{(\rightarrow)}$ is generated for the right hop trial; if $r^{(\rightarrow)} \leq P_{zone}^{(\rightarrow)}$ and the neighboring site is empty, the ion moves right.

2. Similarly, a random number $r^{(\leftarrow)}$ is compared to $P_{zone}^{(\leftarrow)}$ for left movement.

3. Movement is only allowed if the target position is unoccupied and within the device boundaries.

The movement rules also account for spatial constraints imposed by the current ion occupancy. As a result, regions with higher ion density naturally exhibit reduced mobility due to site blocking, which serves as a discrete analog of space charge limitation.

8. Implicit space charge effects

Although no explicit Poisson equation is solved, the simulation incorporates space charge feedback because:

- The net voltage difference ΔV_{net} used in Eq. (1) depends on how ions redistribute during the simulation.

- Ion accumulation near electrodes reduces the local field in subsequent steps, lowering the drift probability in those regions.

- This creates a dynamic coupling between ionic configuration and movement statistics, mimicking the screening and repulsion observed experimentally.

9. Summary of drift, diffusion, and space charge representation

- Drift: Introduced through the energy gap term proportional to the applied bias.
- Diffusion: Captured via the Boltzmann factor allowing hopping against the field.
- Space charge: handled implicitly through occupancy dependent field updates and site blocking rules.

This combination provides a computationally efficient yet physically grounded way to reproduce experimentally observed ionic behaviors such as relaxation, hysteresis, and retention decay, without resorting to full atomistic simulations.

S2.2 Description of initialization routines for each protocol simulation

Before running any protocol, the user must specify a set of initialization parameters in the configuration file (`user_configurations.yaml`). These parameters determine the experimental conditions, simulation geometry, and time–voltage characteristics for the selected protocol. The initialization stage ensures that all simulations are reproducible and based on clearly defined input conditions.

1. General Configuration Parameters

These parameters are required for all protocol types:

- **Ion Occupancy Fraction (0–100%)** – Defines the proportion of available lattice sites initially occupied by mobile ions. This parameter is derived from the experimental ion concentration, typically expressed as the ratio of ionic species to the ion conducting polymer matrix. It provides a direct mapping from experimental loading levels to the number of cations represented in the simulated device.
- **Temperature (K)** – Operating temperature in Kelvin. Although the current implementation relies on a user defined relaxation time instead of temperature dependent mechanisms, this value is retained for compatibility and for possible future simulations that include thermal effects.
- **Save Results (1 or 0)** – Enables or disables the saving of simulation results to file.
- **Device Dimensions:**
  - *Dimension in y* – Number of parallel rails (rows) in the device.
  - *Dimension in x* – Number of available ion sites (columns) along each rail.
- **Starting Mode (0–100%)** – Specifies the uniformity of the initial ion distribution. A value of 100% indicates fully uniform occupancy, whereas lower values produce more spatial variation.
- **Type of Simulation** – Selection of the simulation protocol:
  1. Current decay due to relaxation of electric polarization
  2. Hysteresis
  3. Learning/forgetting rate
- **Relaxation Time (s)** – The intrinsic timescale over which ionic rearrangements occur.
- **Effective Voltage Difference Factor** – Scaling factor applied to the applied voltage to account for charge accumulation effects.

2. Decay of current due to relaxation of electric polarization

When *Current decay* is selected, the following parameters must be specified:

- **Constant Voltage (V)** – Voltage applied during the relaxation phase.
- **Polarization Time (s)** – Duration of the pre-polarization stage before the relaxation begins.
- **Polarization Voltage (V)** – Voltage used during the polarization stage.
- **Total Experiment Time (s)** – Duration of the entire relaxation experiment.
- **Maximum and Minimum Voltage (V)** – Define the operating range; in constant-voltage decay, these values may be used for later analysis.

3. Hysteresis (Variable Voltage)

For the *Hysteresis* protocol, the user specifies:

- **Maximum Voltage (V)** – Peak voltage during the sweep.
- **Minimum Voltage (V)** – Lowest voltage during the sweep.
- **Sweep Rate (V/s)** – Voltage change rate that defines the period of the sweep cycle. This parameter determines the total duration of the experiment according to the voltage range.

4. Learning / Forgetting Rate

In this protocol, the applied voltage consists of pulses with varying amplitude and polarity. Required parameters are:

- **Maximum Voltage (V)** – Pulse amplitude during the “learning” phase.
- **Minimum Voltage (V)** – Pulse amplitude during the “forgetting” phase.
- **Time for Maximum Pulses (s)** – Duration of the learning phase.
- **Time for Minimum Pulses (s)** – Duration of the forgetting phase.
- **Baseline Pulse** – Offset voltage applied between pulses.
- **Pulse Shape** – Either *Triangular* or *Rectangular*, defining the waveform within each pulse cycle.
- **Pulse Frequency (Hz)** – Number of pulses per second.

5. Role of Initialization

The initialization routine reads these values in the order they appear in the configuration file and constructs the internal `config` structure. This structure defines:

- The spatial arrangement and number of ions (`dimension_x`, `dimension_y`, `ion_fraction`).
- The timescale and number of simulation steps (`relaxation_time`, `total_time`).
- The complete voltage vs. time profile for the selected protocol.

By providing a complete and well-defined set of parameters, the user ensures that the simulation can be exactly reproduced and that comparisons between different experiments are valid.

S3. Conversion of Ionic Distributions to Conductance/Current Variables

To enable direct comparison between simulated ion dynamics and experimental observables, we developed a function that converts the ionic occupation data into quantities proportional to conductance and current. The procedure is based on tracking the fraction of ions located in specific deciles of the simulated lattice, which are assumed to dominate charge transport pathways during device operation. This choice reflects the experimental observation that conductance in polymer-based memristive devices is strongly correlated with ionic accumulation near interfaces and preferential migration channels.

For hysteresis simulations, the algorithm identifies the fraction of ions located in the first and tenth deciles of the lattice, depending on the sign of the applied bias. When the voltage is positive, the lowest decile (near one electrode) is used, while under negative voltage the uppermost decile is considered. This decile dependent ionic ratio is normalized by the total ion number and multiplied by the applied time vector, yielding a trajectory that can be directly related to device conductance and current–voltage characteristics.

For relaxation decay simulations, the function extracts the ionic ratio from the first decile as a function of time, which represents the progressive redistribution of ions after a bias pulse. The simulated data are normalized to match the range of experimental delay time curves obtained from independent measurements, enabling a consistent comparison of decay dynamics between simulation and experiment.

Finally, in general simulation modes, the function records the ionic ratio across the selected deciles together with the applied voltage, producing datasets that can be exported for post-processing or fitting to experimental traces. In all cases, the resulting output provides three data streams: (i) the experimental ion ratio for direct reference, (ii) the original simulated ionic ratio, and (iii) a normalized version rescaled to the experimental range. This workflow allows systematic conversion of raw ionic density profiles into transport related observables, bridging the gap between microscopic stochastic simulations and macroscopic electrical measurements.

S4. CPU–GPU performance and energy efficiency comparison

To quantitatively assess the benefits of GPU acceleration, we benchmarked the JAX implementation of the simulation on both CPU and GPU backends using identical workloads. Tables S2 and S3 summarize the runtime, computational throughput, and energy metrics for increasing numbers of simulated rails.

Overall, the GPU consistently achieved higher throughput and lower energy consumption across all test cases. The performance speedup ranged from approximately 1.3× for small scale simulations (500 rails) to about 17× for large scale workloads (128,000 rails). Correspondingly, the energy efficiency improved significantly, with up to sevenfold energy savings at higher scales. These improvements arise from the higher degree of parallelization and better computational intensity per watt of modern GPUs, particularly when combined with JAX's just-in-time (JIT) compilation and vectorized operation support.

Rails	**CPU time**	**GPU time**	**CPU steps**	**GPU steps**	**CPU rails**	**GPU rails**	**Speedup**
	(s)	(s)	(steps/s)	(steps/s)	(rails/s)	(rails/s)	
500	125	94	1498	1991	748800	995745	1.3
1000	210	100	891	1872	891429	1872000	2.1
2000	401	122	467	1534	933666	3068852	3.3
4000	866	162	216	1156	864665	4622222	5.3
8000	1987	224	94	836	753699	6685714	8.9
16000	4130	359	45	521	725230	8343175	11.5
32000	9277	635	20	295	645726	9433701	14.6
64000	18932	1165	10	161	632833	10283948	16.3
128000	37288	2224	5	84	642609	10774101	16.8

Supplementary Table S2. Performance comparison between CPU and GPU implementations for increasing numbers of rails. The GPU consistently achieves higher throughput and speedup as the workload scales.

Rails	CPU power (W)	GPU power (W)	CPU energy (Wh)	GPU energy (Wh)	CPU energy/rail (mWh)	GPU energy/rail (mWh)	Energy savings
500	20.24	31.4	0.70	0.82	1.41	1.64	0.9
1000	19.57	32.8	1.14	0.91	1.14	0.91	1.3
2000	18.87	32.53	2.10	1.10	1.05	0.55	1.9
4000	18.46	32.75	4.44	1.47	1.11	0.37	3.0
8000	17.32	34.8	9.56	2.17	1.19	0.27	4.4
16000	17.29	36.89	19.84	3.68	1.24	0.23	5.4
32000	18.76	38.81	48.34	6.85	1.51	0.21	7.1
64000	18.03	43.03	94.82	13.92	1.48	0.22	6.8
128000	17.95	43.92	185.92	27.13	1.45	0.21	6.9

Supplementary Table S3. Energy and power comparison between CPU and GPU implementations. GPU acceleration significantly reduces energy per rail and overall energy consumption as problem size increases.

S5. Model Validation and Parameter Dependence

S5.1 Effect of Rail Number on Statistical Noise

Due to the stochastic nature of KMC simulations, individual realizations of the current relaxation exhibit statistical fluctuations. To quantify how these fluctuations depend on model resolution, we performed multiple independent simulations for increasing numbers of rails and analysed the variance of the resulting relaxation curves. Each rail contributes independently to the total current, so increasing the rail number effectively averages out uncorrelated fluctuations. As a consequence, the relaxation curves become progressively smoother and more reproducible as the number of rails increases (Figure S1). This behavior reflects the expected reduction of statistical noise with increasing ensemble size.

For each rail number, we computed the mean relaxation curve and the standard deviation across independent runs at each time point. Table S4 and Figure S2 summarize the maximum standard deviation observed over the full time window. While low resolution models exhibit significant variability, the statistical spread decreases rapidly with increasing rail number. For instance, for simulations with 16 000 rails, the maximum standard deviation of the normalized current remains below 0.1 a.u. at all times. This level of fluctuation is negligible compared to typical experimental uncertainties, indicating that simulations with high rail numbers yield statistically robust and reproducible results. These findings justify the choice of rail numbers adopted in the main text and demonstrate that the reported relaxation behavior is not an artifact of stochastic noise.

	20	40	60	80	100	120	140	160	180	200	220	240	260	280
500	0.399	0.457	0.467	**0.546**	0.476	0.414	0.441	0.464	0.436	0.447	0.374	0.332	0.333	0.340
1000	0.284	0.288	0.350	0.373	0.330	0.289	0.341	0.352	**0.389**	0.316	0.331	0.280	0.286	0.241
2000	0.223	0.215	0.233	0.240	0.253	0.218	0.207	0.235	0.244	**0.254**	0.217	0.185	0.190	0.164
4000	0.154	0.182	**0.204**	0.185	0.183	0.168	0.171	0.160	0.169	0.179	0.156	0.138	0.151	0.116
8000	0.119	0.124	0.134	0.124	0.128	0.144	0.134	0.144	0.144	**0.155**	0.143	0.126	0.113	0.094
16000	0.082	0.093	0.092	0.089	0.098	**0.099**	0.090	0.088	0.092	0.084	0.089	0.083	0.072	0.073

Supplementary Table S4. Standard deviation of relaxation curves among independent runs as a function of measured current (columns) and number of rails (rows). Each value is obtained from 30 independent replicas by computing the variance of the current over a time window of $t \pm 10\,\mathrm{s}$ and then averaging across replicas.

S5.2 Current relaxation and influence of relaxation time

When the polarization voltage is removed, the driving electric field that sustains ionic displacement across the nanodevice vanishes. As a result, mobile ions gradually relax back toward their equilibrium distribution within the material. This ionic redistribution reduces the internal electric field and charge imbalance responsible for the measured current. Consequently, the current decays over time until reaching a steady-state value determined by the equilibrium ionic configuration, reflecting the intrinsic relaxation dynamics of the device.

Additionally, as shown in Figure S3, the visual noise in the simulated current decreases with increasing relaxation time. Longer relaxation times allow the ionic and electronic variables to evolve more smoothly, effectively filtering out high frequency fluctuations and producing cleaner, more stable decay profiles. This behavior highlights the damping effect of slower ion dynamics on transient current noise within the nanodevice.

It is important to emphasize that the experimental dataset used in the convergence study was generated as part of the work by Prado-Socorro *et al.* [1]. The measurements correspond to polymer-based memristive devices (device NM_V146), where the electrical response was recorded after the application of voltage pulses followed by variable delay times. For each delay time, the ratio between the measured current after the delay and the reference current was extracted, providing a quantitative measure of the relaxation and memory retention behavior of the device. In the present work, only the delay time and the corresponding current ratio (Table S5) were used for comparison with the simulation results, enabling a direct assessment of the convergence and temporal scaling of the model against experimentally observed trends.

Device name	Day	Pixel	Curve	Delay time (s)	Current ratio
NM_V146	3	R3	0	1	12.253
NM_V146	3	R3	1	2	13.530
NM_V146	3	R3	2	5	11.703
NM_V146	3	R3	3	10	8.462
NM_V146	3	R3	4	30	5.203
NM_V146	3	R3	5	60	3.628
NM_V146	3	R3	6	180	2.046
NM_V146	3	R3	7	300	1.650

Supplementary Table S5. Experimental dataset extracted from Prado-Socorro *et al.* [1] and used for the convergence study. The table reports the delay time after stimulation and the corresponding current ratio for device NM_V146.

S5.3 Hysteresis loops at different voltage sweep rates

Figure S4 shows the simulated I–V hysteresis loops. At increasing voltage sweep rates, the simulated I–V hysteresis loops exhibit a progressive reduction in current and loop amplitude. This trend arises from the limited response time of the system: faster voltage changes restrict the extent of ionic and electronic rearrangements, thereby diminishing the overall current magnitude and narrowing the hysteresis loops.

S5.4 Relaxation Dynamics of Conductance

Figure S5 shows the time evolution of the conductance for the device under a pulsed voltage waveform, highlighting the effect of different relaxation times, τ. The top panel displays the conductance traces for five different τ values ranging from 0.0005 s to 0.0055 s. Each trace exhibits a characteristic learning (increase) phase during the initial positive voltage pulse, followed by a forgetting (decay) phase once the voltage reverses.

Shaded areas represent the regions under each conductance curve, with transparency adjusted to allow visualization of overlapping curves. As expected, shorter relaxation times lead to a faster rise and decay of the conductance, while longer relaxation times result in more gradual changes, consistent with a slower adaptation to the applied voltage.

The bottom panel shows the voltage waveform applied to the device, which is a high frequency, square-like signal alternating between positive and negative values. The way the conductance response follows this waveform highlights the device's temporal dynamics and memory behavior under rapid voltage changes.

[1] Prado-Socorro CD, Giménez-Santamarina S, Mardegan L, Escalera-Moreno L, Bolink HJ, Cardona-Serra S, et al. Polymer-based composites for engineering organic memristive devices. Adv Electron Mater. 2022 May;8(5):2101192. Available from: https://doi.org/10.1002/aelm.202101192.

[2] Gutiérrez-Finol GM, Giménez-Santamarina S, Hu Z, Rosaleny LE, Cardona-Serra S, Gaita-Ariño A. Lanthanide molecular nanomagnets as probabilistic bits. Npj Comput Mater. 2023 Oct;9(1):196. Available from: https://doi.org/10.1038/s41524-023-01149-7.

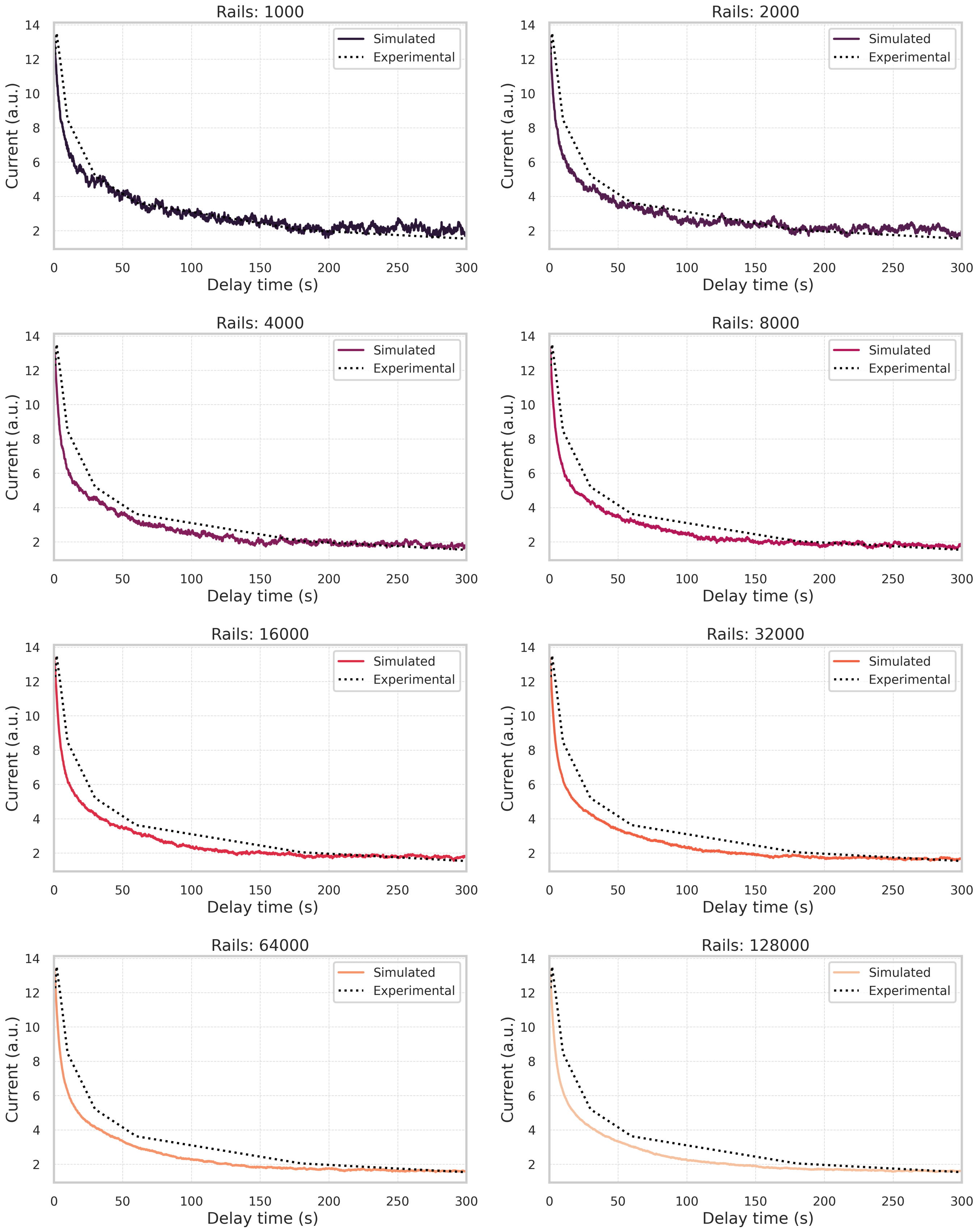

Supplementary Figure S1. Current relaxation as a function of delay time for different numbers of simulated rails (from 1000 to 128000), compared with experimental data. Each panel shows the ensemble averaged simulated current (solid line) and the corresponding experimental response (dotted line). Increasing the number of rails reduces stochastic fluctuations in the simulated signal, leading to progressively smoother relaxation curves while preserving the overall decay dynamics. The improved agreement highlights the role of ensemble averaging in suppressing rail-to-rail noise and revealing the intrinsic relaxation behavior.

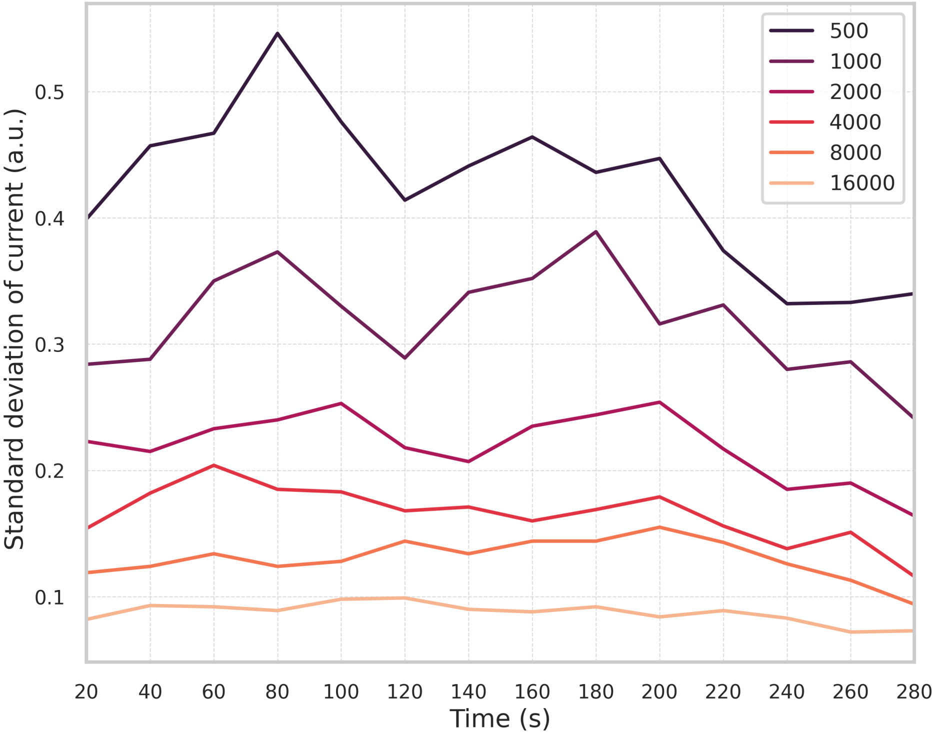

Supplementary Figure S2. Values for the Table S4.

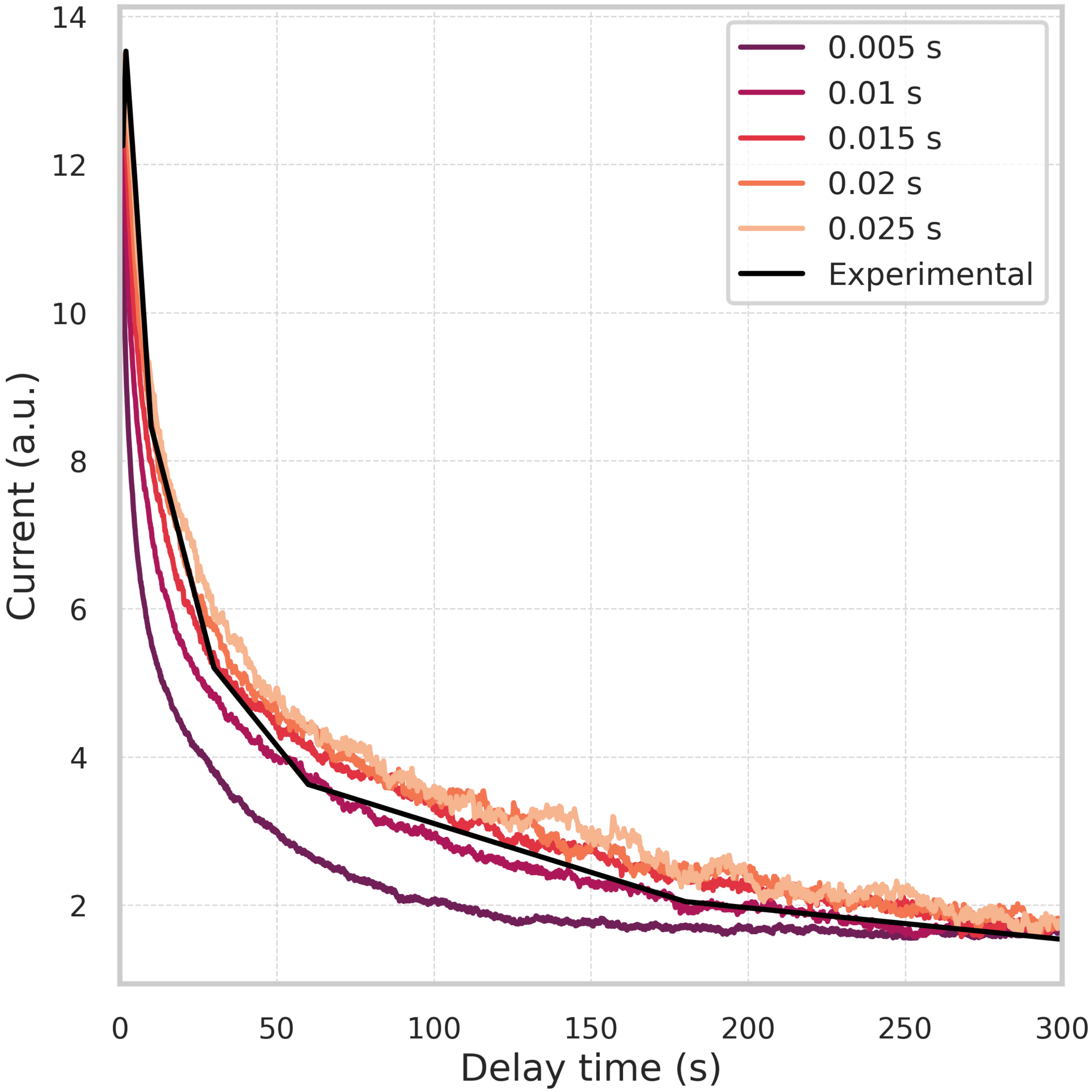

Supplementary Figure S3. Simulated relaxation decay curves obtained at different relaxation times (0.005–0.025 s), compared with experimental data (solid black line). Each simulated curve corresponds to a distinct relaxation parameter in the model. Shorter relaxation times produce faster decay dynamics and lower steady-state currents, while longer times lead to a slower relaxation toward equilibrium. The experimental trace serves as a reference for evaluating the temporal response of the simulated system.

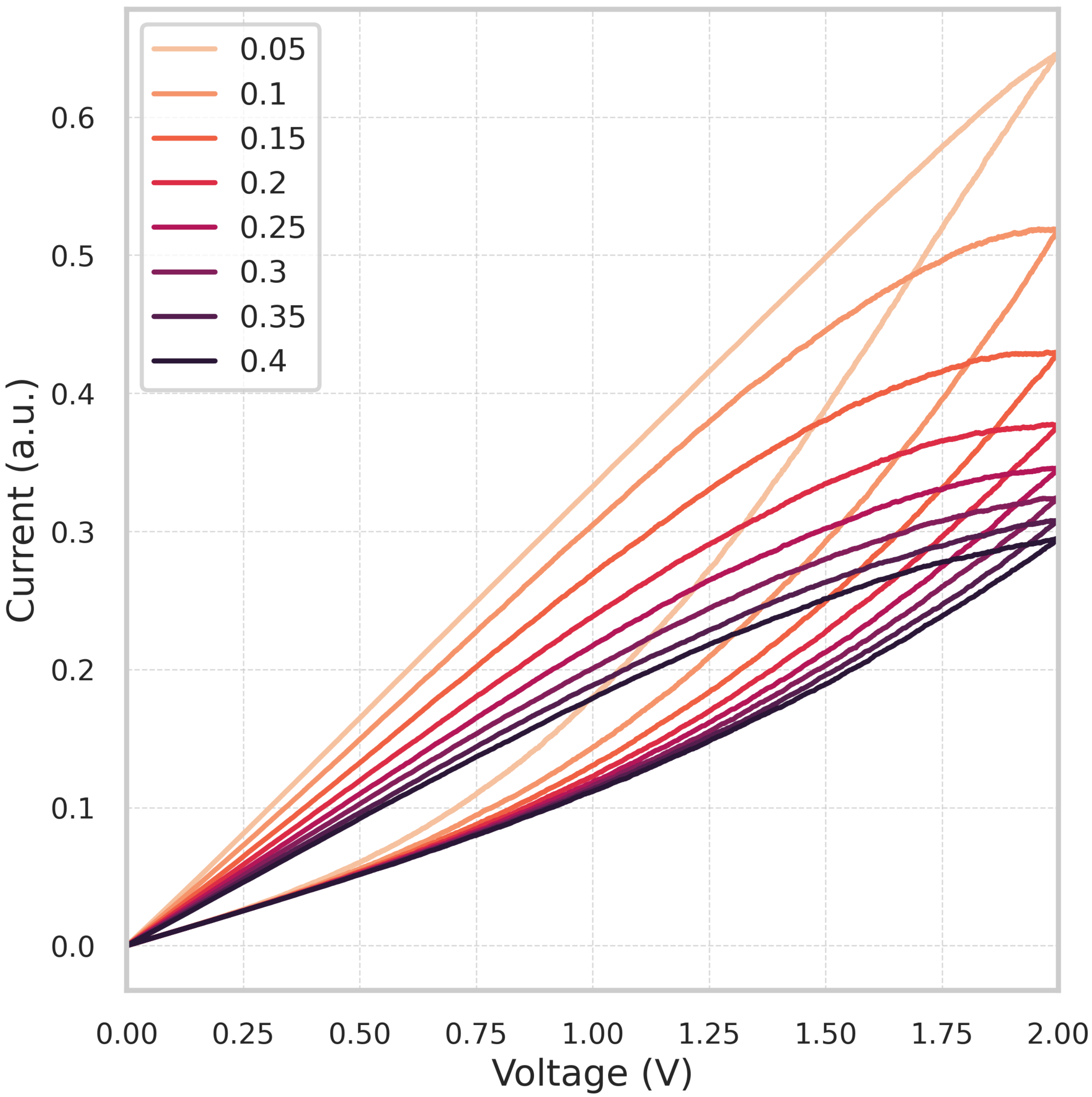

Supplementary Figure S4. Simulated I–V hysteresis loops obtained at different voltage sweep rates (0.05–0.4 V/s). Each curve corresponds to a specific sweep rate, indicated in the legend. As the sweep rate increases, the overall current decreases, resulting in smaller loop amplitudes. This behavior reflects the dynamic response of the system, where faster sweeps reduce the time available for ionic or electronic rearrangements.

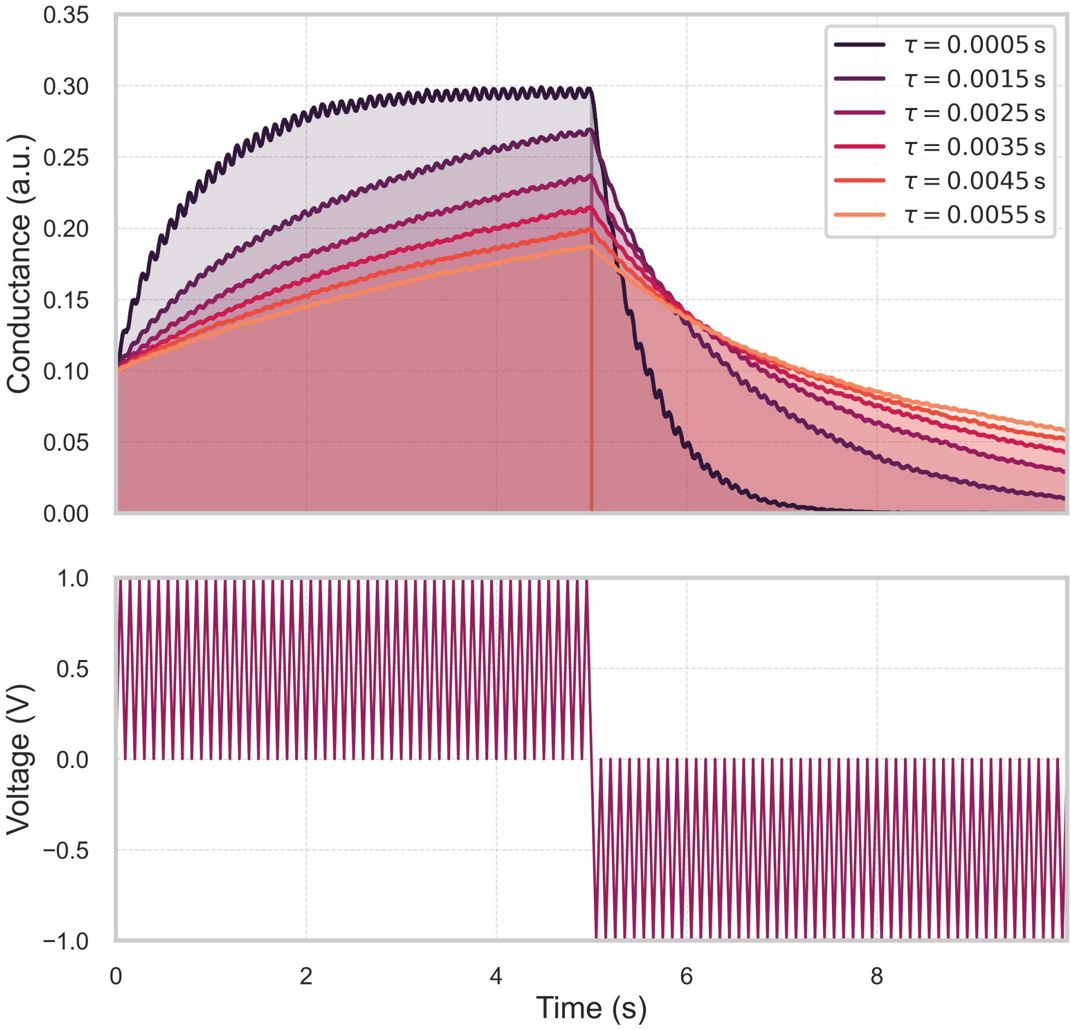

Supplementary Figure S5. Time evolution of conductance (top) for six different relaxation times, τ, and corresponding applied voltage waveform (bottom). Shaded areas highlight the integrated conductance during the learning and forgetting phases.